



1 **Increased Importance of Aerosol-Cloud Interaction for Surface**
2 **PM_{2.5} Pollution Relative to Aerosol-Radiation Interaction in**
3 **China With the Anthropogenic Emission Reduction**

4
5 Da Gao^{1,2}, Bin Zhao^{1,2,*}, Shuxiao Wang^{1,2}, Yuan Wang³, Brian Gaudet⁴, Yun
6 Zhu⁵, Xiaochun Wang^{1,2}, Jiewen Shen^{1,2}, Shengyue Li^{1,2}, Yicong He^{1,2}, Dejjia
7 Yin^{1,2}, Zhaoxin Dong^{1,2}

8
9 ¹State Key Joint Laboratory of Environment Simulation and Pollution Control,
10 School of Environment, Tsinghua University, 100084 Beijing, China

11 ²State Environmental Protection Key Laboratory of Sources and Control of Air
12 Pollution Complex, Beijing, 100084, China

13 ³Department of Earth, Atmospheric, and Planetary Sciences, Purdue University,
14 West Lafayette, IN, USA,

15 ⁴Pacific Northwest National Laboratory, Richland, Washington, USA

16 ⁵Guangdong Provincial Key Laboratory of Atmospheric Environment and
17 Pollution Control, College of Environment and Energy, South China University
18 of Technology, Guangzhou Higher Education Mega Center, Guangzhou, 510006,
19 China

20 *Correspondence to: Bin Zhao (bzhao@mail.tsinghua.edu.cn)

21
22 **Abstract:** Surface fine particulate matter (PM_{2.5}) pollution can be enhanced by



23 feedback processes induced by aerosol-radiation interactions (ARI) and aerosol-
24 cloud interactions (ACI). Many previous studies have reported enhanced $PM_{2.5}$
25 concentration induced by ARI and ACI for episodic events in China. However,
26 few studies have examined the changes in the ARI- and ACI-induced $PM_{2.5}$
27 enhancements over a long period, though the anthropogenic emissions have
28 changed substantially in the last decade. In this study, we quantify the ARI- and
29 ACI-induced $PM_{2.5}$ changes for 2013–2021 under different meteorology and
30 emission scenarios using the Weather Research and Forecasting model with
31 Chemistry (WRF-Chem) and investigate the driving factors for the changes. Our
32 results show that in January 2013, when China suffered from the worst $PM_{2.5}$
33 pollution, the $PM_{2.5}$ enhancement induced by ARI in eastern China ($5.59 \mu\text{g m}^{-3}$)
34 is larger than that induced by ACI ($3.96 \mu\text{g m}^{-3}$). However, the ACI-induced
35 $PM_{2.5}$ enhancement shows a significantly smaller decrease ratio (51%) than the
36 ARI-induced enhancement (75%) for 2013–2021, making ACI more important
37 for enhancing $PM_{2.5}$ concentrations in January 2021. Our analyses suggest that
38 the anthropogenic emission reduction plays a key role in this shift. Owing to only
39 anthropogenic emission reduction, the ACI-induced $PM_{2.5}$ enhancement
40 decreases by 43% in January and 57% in July, lower than the decrease ratio of
41 the ARI-induced enhancement (57% in January and 67% in July). The primary
42 reason for this phenomenon is that the decrease of ambient $PM_{2.5}$ for 2013–2021
43 causes a disproportionately small decrease of liquid water path (LWP) and
44 increase of cloud effective radius (Re) under the condition of high $PM_{2.5}$



45 concentration, therefore the surface solar radiation attenuation (and hence
46 boundary layer height reduction) caused by ACI decreases slower than that
47 caused by ARI. Moreover, the lower decrease ratio of the ACI-induced $PM_{2.5}$
48 enhancement is dominated by the lower decrease ratio of ACI-induced secondary
49 $PM_{2.5}$ component enhancement, which is additionally caused by smaller decrease
50 ratio of the air temperature reduction and relative humidity (RH) increase. Our
51 findings reveal that with the decrease of ambient $PM_{2.5}$, the ACI-induced $PM_{2.5}$
52 enhancement inevitably becomes more important, which needs to be considered
53 in the formulation of control policies to meet the national $PM_{2.5}$ air quality
54 standard.

55

56 **1. Introduction**

57 Aerosol-radiation interaction (ARI) and aerosol-cloud interaction (ACI) are
58 important ways for aerosols to influence the climate (Rosenfeld et al., 2014;
59 Seinfeld et al., 2016; Liu et al., 2018; Bellouin et al., 2020; Forster et al., 2021).
60 The ARI represents the direct scattering and absorption of solar and infrared
61 radiation by atmospheric aerosols; the ACI denotes the modification effects on
62 the lifetime, physical and optical properties of clouds by atmospheric aerosols.

63 Previous studies have documented that both ARI and ACI have important
64 contributions to inhibiting the planetary boundary layer height (PBLH), cooling
65 the near-surface air temperature, and increasing the relative humidity (RH) (Wang
66 et al., 2014; Ding et al., 2016; Liu et al., 2018). Moreover, ACI has extra
67 contributions to changing precipitation and cloud chemistry (Zhao et al., 2017;



68 Zhang et al., 2018). These feedbacks and changes are mostly conducive to
69 increasing the haze severity (Wang et al., 2015; Zhang et al., 2018; Liu et al.,
70 2018; Zhou et al., 2019; Zhang et al., 2020; Xiong et al., 2022; Lin et al., 2022).
71 So far, numerous studies have evaluated the fine particulate matter ($PM_{2.5}$)
72 enhancements caused by the decreases of downward shortwave radiation at the
73 surface (SWDOWN), PBLH, near-surface air temperature and precipitation, and
74 by the increase of RH, especially during the severe $PM_{2.5}$ pollution in China (Le
75 et al., 2020). Zhang et al. (2015) and Zhang et al. (2018) quantified that the ARI
76 caused the $PM_{2.5}$ increase by $8.3 \mu\text{g m}^{-3}$ in 2013 and $4.0 \mu\text{g m}^{-3}$ in 2014. However,
77 both positive and negative contributions of ACI to the $PM_{2.5}$ have been revealed
78 (Forkel et al., 2012; 2015; Kong et al., 2015; Zhang et al., 2015; Zhang et al.,
79 2018). Zhao et al. (2017) pointed out that the negative contribution of ACI shown
80 in some studies (Gustafson et al., 2007; Gong et al., 2015) is due to the relatively
81 high prescribed values of cloud droplet number concentration (CDNC) or cloud
82 condensation nuclei (CCN), which could not represent a rather clean condition.
83 Besides, there might be a discrepancy between the enhancements induced by ARI
84 and ACI for primary and secondary $PM_{2.5}$ components. The primary $PM_{2.5}$
85 components are mainly influenced by physical transport, while the secondary
86 $PM_{2.5}$ components are also affected by chemical formation and decomposition.
87 The lower air temperature and higher RH can help to condense gas precursors
88 into secondary aerosol particles (Donahue et al., 2012) and strengthen aqueous
89 and heterogeneous reactions (Liu et al., 2018). On the contrary, Wu et al. (2020)



90 pointed out that the ARI may also suppress the formation of secondary aerosol
91 because the atmospheric oxidizing capacity and photolysis rate can be changed
92 during the scattering and absorbing of solar radiation. Therefore, not all changes
93 of meteorological factors are conducive to the increase of secondary $PM_{2.5}$, and
94 these positive and negative contributions would influence the variations of
95 primary and secondary $PM_{2.5}$ components. In a word, although the ARI and ACI
96 processes mostly lead to a net $PM_{2.5}$ increase, the relative increasing rates of
97 different aerosol components are fairly complex due to various physical and
98 chemical processes.

99 In recent years, the Chinese government has successively proclaimed the
100 policies of “Air pollution prevention and control action plan” and “Three-year
101 action plan to win the blue sky defense war”, including the promotion of ultra-
102 low emission technologies in industrial sectors, the implementation of traffic
103 restriction policies, and the transition from coal to gas in residential cooking. As
104 a result, the annually averaged $PM_{2.5}$ concentrations in Beijing-Tianjin-Hebei
105 region, Yangtze River Delta (YRD) and Pearl River Delta have been reduced by
106 39.6%, 34.2%, and 27.7% from 2013 to 2017, respectively (Wang et al., 2017;
107 Ding et al., 2019a). Meanwhile, sulfate and organic components have respectively
108 decreased by 76% and 70 % in the North China Plain (NCP) (Wang et al., 2019).
109 Considering the sharp anthropogenic emission reduction and $PM_{2.5}$ concentration
110 decrease, Moch et al. (2022) found that the decrease of mean $PM_{2.5}$ concentration
111 weakened the cloud-snowfall-albedo feedback induced by the aerosol semi-direct



112 effect. For air quality, Zhang et al. (2022) found that the decrease of black carbon
113 (BC) would reduce the enhanced $PM_{2.5}$ concentration induced by the ARI by 1.8
114 $\mu\text{g m}^{-3}$ in January and 0.3 $\mu\text{g m}^{-3}$ in July.

115 However, none of the previous studies have systematically evaluated the
116 changes in enhanced $PM_{2.5}$ concentrations through ARI and ACI in China at the
117 long-term scale. Besides, the driving force and physical mechanisms for the
118 changes are also yet to be explored. In this study, we try to investigate the
119 enhanced $PM_{2.5}$ concentrations induced by ARI and ACI in 2013 over China, the
120 impact of the changes in the meteorological background and anthropogenic
121 emission from 2013 to 2021 on ARI- and ACI-induced $PM_{2.5}$ enhancements and
122 its components. Furthermore, the causes of $PM_{2.5}$ enhancement changes are
123 analyzed.

124

125 **2. Model and experimental design**

126 **2.1 Model configuration**

127 The Weather Research and Forecasting model with Chemistry (WRF-Chem)
128 version 4.2 has been used in this study. The model domain covers the whole land
129 area of China with a horizontal resolution of $27\text{ km} \times 27\text{ km}$. There are 24 vertical
130 layers from surface to 50 hPa, with denser layers in the planetary boundary layer
131 (PBL). Major physical options used in the model include the Morrison double-
132 moment scheme (Morrison et al., 2009), the Rapid Radiative Transfer Model for
133 GCMs (RRTMG) shortwave and longwave radiative transfer schemes (Iacono et



134 al., 2008), the Eta similarity surface-layer scheme (Janjic et al., 1994), the Noah
135 land-surface model with multiple parameterization options (Niu et al., 2011), the
136 Bougeault and Lacarrere PBL scheme (Bougeault et al., 1989), and the Grell-
137 Freitas ensemble cumulus scheme (Grell et al., 2014). For chemistry, we employ
138 the SAPRC-99 (Statewide Air Pollution Research Center mechanism, version
139 1999) as the gas-phase chemistry mechanism (Carter et al., 2000). The aerosol
140 module used in the study is the Model for Simulating Aerosol Interactions and
141 Chemistry (MOSAIC) (Zaveri et al., 2008), which includes all major aerosol
142 processes and represents the aerosol size distribution with 8 size bins. The
143 MOSAIC also incorporates the one-dimensional Volatility Basis Set (VBS)
144 framework that improves the simulation of secondary organic aerosol
145 (Shrivastava et al., 2011). Rates for photolytic reactions are calculated using the
146 Fast-J photolysis rate scheme (Wild et al., 2000). The meteorological initial and
147 boundary conditions are derived from the National Centers for Environmental
148 Prediction Final Analysis reanalysis data with resolutions of $1.0^{\circ} \times 1.0^{\circ}$ and 6 h
149 (<http://rda.ucar.edu/datasets/ds083.2/>). The chemical initial and boundary
150 conditions are acquired from the simulation results of the National Center for
151 Atmospheric Research's Community Atmosphere Model with Chemistry (CAM-
152 Chem, before 2020, <https://www.acom.ucar.edu/cam-chem/cam-chem.shtml>) and
153 the Whole Atmosphere Community Climate Model (WACCM, after 2020,
154 <https://www.acom.ucar.edu/waccm/download.shtml>) with resolutions of $0.94^{\circ} \times$
155 1.25° and 6 h.



156 The anthropogenic emission data in China for 2013-2021 are obtained from
157 the ABaCAS-EI (Air Benefit and Cost and Attainment Assessment System-
158 Emission Inventory) developed by Tsinghua University (Li et al., 2023). The
159 emission data in other countries are obtained from the IIASA emission inventory
160 for 2015 (Zheng et al., 2019; Gao et al., 2020). The biogenic emission is
161 calculated online by the Model of Emissions of Gases and Aerosols from Nature
162 (MEGAN) v2.04 (Guenther et al., 2006). The dust emission is calculated online
163 by the Goddard Chemistry Aerosol Radiation and Transport (GOCART) model
164 coupled with the MOSAIC aerosol schemes. (Zhao et al., 2010; 2013)

165 To account for the physical processes of aerosol-radiation-cloud feedback
166 on meteorological factors and $PM_{2.5}$, the four-dimensional data assimilation
167 (FDDA) is not utilized in our simulations. Aerosol optical depth, single scattering
168 albedo, and asymmetry factors are calculated based on the Lorenz-Mie theory as
169 a function of wavelength and three-dimensional location (Fast et al., 2006). Then,
170 the aerosol optical properties are transferred to the RRTMG radiation scheme to
171 calculate the impact of aerosol on the radiation balance (Iacono et al., 2008). As
172 for the ACI, activated aerosols are calculated by the Abdul-Razzak and Ghan
173 scheme (Abdul-Razzak & Ghan, 2002) and are then coupled with the Morrison
174 two-moment cloud microphysics scheme (Morrison et al., 2009). The prognostic
175 cloud water content calculated by the Morrison scheme is input into the RRTMG
176 scheme for the radiative transfer calculation. It should be noted that the prognostic
177 aerosol does not influence cumulus clouds and ice nucleation in the model.



178

179 **2.2 Experimental design**

180 As described in the introduction, the purpose of this study is to quantify the
181 contributions of ARI and ACI to $PM_{2.5}$ concentrations under different emission
182 scenarios. The simulation periods are January and July, 2013 and 2021,
183 representing winter and summer, respectively.

184 As shown in Table 1, the enhanced $PM_{2.5}$ concentration induced by ARI and
185 ACI could be obtained via comparing the simulation results with ARI or ACI
186 turned on or off. By setting the ‘aer_ra_feedback’ to 0 in the model, the ARI could
187 be turned off, which means that the interaction between aerosol and radiation is
188 prevented. The ACI could be turned off through prescribing the CDNC of 25 cm^{-3}
189 in the microphysical scheme, which represents average level in the pristine air
190 (Bennartz et al., 2007). For example, the 13M13E_B, 13M13E_NR and
191 13M13E_NRC shown in Table 1 represent the cases with ARI and ACI effects,
192 without ARI effect, and without ARI and ACI effects in 2013, respectively. The
193 ARI-induced $PM_{2.5}$ enhancement could be acquired by comparing the results of
194 13M13E_B and 13M13E_NR; the ACI-induced $PM_{2.5}$ enhancement could be
195 obtained by comparing the results of 13M13E_NR and 13M13E_NRC.

196

197 **Table 1. Case definition under different meteorological backgrounds and**
198 **anthropogenic emissions with ARI or ACI turned on or off.**

Case	Meteorology	Emission	ARI	ACI
------	-------------	----------	-----	-----



13M13E_B	Jan & Jul, 2013	Jan & Jul, 2013	on	on
13M13E_NR	Jan & Jul, 2013	Jan & Jul, 2013	off	on
13M13E_NRC	Jan & Jul, 2013	Jan & Jul, 2013	off	off
21M13E_B	Jan & Jul, 2021	Jan & Jul, 2013	on	on
21M13E_NR	Jan & Jul, 2021	Jan & Jul, 2013	off	on
21M13E_NRC	Jan & Jul, 2021	Jan & Jul, 2013	off	off
21M21E_B	Jan & Jul, 2021	Jan & Jul, 2021	on	on
21M21E_NR	Jan & Jul, 2021	Jan & Jul, 2021	off	on
21M21E_NRC	Jan & Jul, 2021	Jan & Jul, 2021	off	off

199

200 In order to obtain the changes of the ARI- and ACI-induced $PM_{2.5}$
201 enhancements from 2013 to 2021 caused by the variation of meteorological
202 background and by the reduction of anthropogenic emission, the control
203 experiments (21M13E; three experiments: with ARI and ACI turned on, with ARI
204 turned off and ACI turned on, and with ARI and ACI turned off) are designed
205 with the meteorological background in 2021 and the anthropogenic emission in
206 2013. In the following, the 13M13E, 21M13E and 21M21E represent the cases
207 with meteorological background and anthropogenic emission in 2013,
208 meteorological background in 2021 and anthropogenic emission in 2013, and
209 meteorological background and anthropogenic emission in 2021, respectively.
210 Taking the ARI for example, the change of the ARI-induced $PM_{2.5}$ enhancement
211 from the variation of meteorological background is obtained by subtracting the



212 ARI-induced $PM_{2.5}$ enhancement in the 13M13E from that in the 21M13E [Eq.
213 (1)]; the change in the ARI-induced $PM_{2.5}$ enhancement from the reduction of
214 anthropogenic emission is obtained by subtracting the ARI-induced $PM_{2.5}$
215 enhancement in the 21M13E from that in the 21M21E [Eq. (2)]. The calculations
216 for the ACI-induced $PM_{2.5}$ enhancement are similar, as shown in Eqs. (3) and (4).
217

$$ARI_{met} = (21M13E_B - 21M13E_NR) - (13M13E_B - 13M13E_NR), \quad (1)$$

$$ARI_{emi} = (21M21E_B - 21M21E_NR) - (21M13E_B - 21M13E_NR), \quad (2)$$

$$ACI_{met} = (21M13E_NR - 21M13E_NRC) - (13M13E_NR - 13M13E_NRC), \quad (3)$$

$$ACI_{emi} = (21M21E_NR - 21M21E_NRC) - (21M13E_NR - 21M13E_NRC), \quad (4)$$

218 where the ARI_{met} (ACI_{met}) and ARI_{emi} (ACI_{emi}) represent the changes of the
219 enhanced $PM_{2.5}$ concentration induced by the ARI (ACI) from 2013 to 2021
220 caused by the variation of meteorological background and reduction of
221 anthropogenic emission, respectively.

222

223 **2.3 Model evaluation**

224 To determine the accuracy and reliability of simulation results, the
225 13M13E_B and 21M21E_B simulations (Table 1) are verified by using the



226 observations. The variables checked in the evaluation contain the concentration
227 and components of surface $PM_{2.5}$ and the meteorological factors, including air
228 temperature (T2) and water vapor mixing ratio (Q2) at 2 m, wind speed (WS10)
229 and wind direction (WD10) at 10 m, as well as cloud fraction (CF) and liquid
230 water path (LWP).

231 Simulated temperature, wind, and water vapor are compared with the
232 observations from the National Climate Data Center (NCDC,
233 <http://www.ncdc.noaa.gov/>). The evaluation shows that the absolute errors for T2,
234 WS10 and Q2 are respectively less than $1^{\circ}C$, 1 m s^{-1} and 0.1 g kg^{-1} (Table S1),
235 and those for WD10 are near or less than 10° . For the simulation utilizing the
236 FDDA, the benchmarks of biases proposed by Emery et al. (2001) are $0.7^{\circ}C$, 0.6
237 m s^{-1} , 1.0 g kg^{-1} and 20° for the T2, WS10, Q2 and WD10, respectively. The
238 biases of the T2 and WS10 in our simulations have exceeded the benchmarks,
239 while they are still similar to or smaller than in most previous WRF-Chem
240 applications without FDDA over East Asia (Zhang et al., 2015; Zhao et al., 2017).

241 Simulated CF and LWP are compared with the data from the Moderate-
242 resolution Imaging Spectroradiometer (MODIS) aboard the Terra satellite
243 (<http://ladsweb.nascom.nasa.gov/data/search.html>). Overall, the CF and LWP
244 simulations are in good agreement with the observations (Figs. S1 and S2). The
245 high values of observed CF and LWP primarily appear in the south of China in
246 January 2013 and 2021, and high value of CF also occurs in the NCP region. The
247 high values of CF and LWP in the south of China could be reproduced in the



248 simulation, while the CF in NCP region is slightly underestimated, which could
249 be owing to imperfect cloud parameterization scheme in the model or
250 uncertainties in the retrieval of MODIS datasets. In July 2013 and 2021, part of
251 high value area of observed LWP and most high value area of observed CF appear
252 in the southwestern China and the east coast of China, which also could be
253 captured by the simulation. In addition, high LWP also appears in Gansu and
254 Sichuan Provinces in July 2013 and in the YRD and Sichuan-Chongqing in July
255 2021, which are both well reproduced. The distributions of low values of
256 observed CF and LWP in January and July of 2013 and 2021 are also well
257 simulated.

258 The simulation of surface $PM_{2.5}$ concentration is compared with the data
259 from the China National Environmental Monitoring Center
260 (<https://quotsoft.net/air/>). The evaluation shows that both the regional average
261 value and spatial distribution of simulated $PM_{2.5}$ concentration are in good
262 agreement with the observational data. As shown in Fig. S3, the biases of regional
263 average $PM_{2.5}$ concentration in January and July of 2013 and 2021 are below 3
264 $\mu\text{g m}^{-3}$ in eastern China. In this study, the eastern China includes most of Chinese
265 provinces except Xinjiang, Xizang, Ningxia, Qinghai, Gansu, Inner-Mongolia
266 and Heilongjiang Provinces, which contains most polluted regions in China. In
267 addition, the distributions of high simulated $PM_{2.5}$ concentration are also
268 consistent with the observations, such as the NCP region, the YRD region, and
269 the Sichuan-Chongqing area.



270 The simulated $PM_{2.5}$ components are also reasonable compared with the
271 observation data, which is from a data sharing platform for the NCP region and
272 its surrounding areas (Wang et al., 2019). Fig. S4 shows the ratios of observation
273 to simulation of ammonium, nitrate, sulfate, BC and organic carbon (OC) in
274 January and July 2021. The results exhibit that almost all the ratios of $PM_{2.5}$
275 components are located between 0.5 and 2.0, while some ratios of sulfate in
276 January and BC in January and July are beyond this range, but not far away. Such
277 minor discrepancies will not cause obvious uncertainty in this research.

278 In summary, the performances of WRF-Chem model on the simulations of
279 air quality and meteorological factors over China are fairly good, and the
280 differences between simulations and observations are reasonable and acceptable.

281

282 **3. Results and discussion**

283 **3.1 The impacts of ARI and ACI feedbacks on the meteorological** 284 **factors and $PM_{2.5}$ concentrations in 2013**

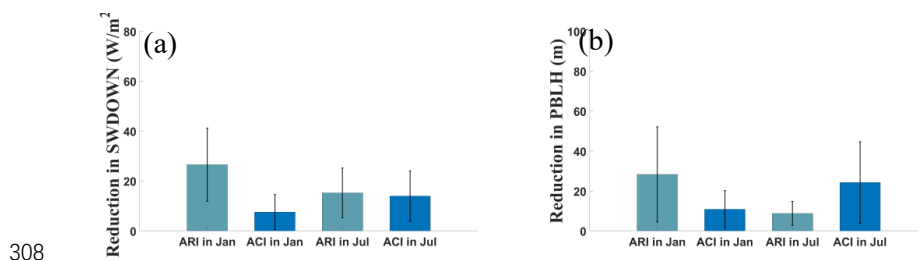
285 We comprehensively discuss the effects of ARI and ACI on the regional
286 meteorological factors and $PM_{2.5}$ concentrations in January and July 2013. Fig. 1
287 shows the impacts of ARI and ACI feedbacks on the SWDOWN, PBLH, T2, RH
288 and $PM_{2.5}$ concentration in January and July 2013. For the ARI, the SWDOWN
289 decreases by 26.55 and 15.28 $W m^{-2}$ in January and July 2013 in eastern China,
290 respectively. Since the incoming solar radiation reaching the ground is reduced
291 by PM, the T2 and PBLH in eastern China further decrease by 0.30 and 0.03°C,

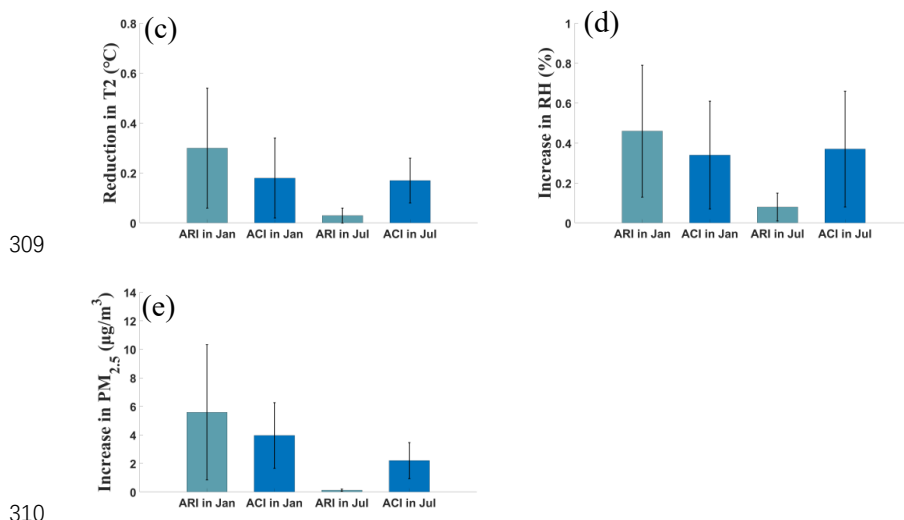


292 and 28.34 and 8.75 m in January and July 2013, respectively. Meanwhile, the RH
293 increases by 0.46% and 0.08% due to the water vapor accumulation in the
294 suppressed planetary boundary layer (Liu et al., 2018). Ultimately, the PM_{2.5}
295 concentration increases by 5.59 and 0.13 $\mu\text{g m}^{-3}$ in eastern China (Fig. 1d). For
296 the ACI, affected by the cloud modified by the aerosol, the SWDOWN, T2 and
297 PBLH decrease by 7.54 and 14.03 W m^{-2} , 0.18 and 0.17 $^{\circ}\text{C}$, and 10.89 and 24.31
298 m, and the RH increases by 0.34% and 0.37% in January and July 2013 in eastern
299 China, respectively. As a result, the PM_{2.5} concentration increases by 3.96 and
300 2.20 $\mu\text{g m}^{-3}$ in eastern China. Fig. 2 shows that the regional averaged values and
301 spatial distributions of PM_{2.5} enhancements induced by ARI and ACI in 2013 are
302 in line with the results of previous studies (Zhao et al., 2017; Zhang et al., 2018).

303 Overall, the enhanced PM_{2.5} concentration induced by ARI is greater than
304 that induced by ACI in January 2013, which is due to the relatively lower LWP
305 in the high PM_{2.5} concentration area. But it shows the opposite situation in July
306 2013, owing to the plentiful cloud in warm July (Zhang et al., 2018).

307





309

310

311 Fig. 1. The regional averaged reductions of (a) downward shortwave radiation at
312 the surface (SWDOWN), (b) planetary boundary layer height (PBLH), (c) 2-m
313 air temperature (T2), and increments of (d) relative humidity (RH) and (e) fine
314 particulate matter (PM_{2.5}) concentration induced by the aerosol-radiative
315 interaction (ARI) and aerosol-cloud interaction (ACI) in January and July 2013
316 in eastern China, the error bars represent the standard deviations for different
317 meteorological factors and PM_{2.5} concentration induced by ARI and ACI in
318 January and July 2013 in eastern China.

319

320 3.2 The shift of the PM_{2.5} enhancements induced by ARI and ACI

321 As discussed in section 3.1, the enhanced PM_{2.5} concentrations induced by
322 ARI and ACI exhibit obvious spatial and seasonal variations in 2013. However,
323 due to the variations of meteorological background and the reduction of
324 anthropogenic emission from 2013 to 2021, their joint and individual impacts on



325 the ARI- and ACI-induced $PM_{2.5}$ enhancements are still unclear. Fig. 2 shows the
326 ARI- and ACI-induced $PM_{2.5}$ enhancements in the experiments of 13M13E,
327 21M13E and 21M21E in January and July.

328 As shown in Fig. 2, from 2013 to 2021, the $PM_{2.5}$ concentration
329 enhancement induced by the ARI in January decreases by 75% (from 5.59 to 1.37
330 $\mu\text{g m}^{-3}$). Zhang et al. (2022) also found that the ARI effect over China weakens
331 during 2013–2017, and the ratio of $PM_{2.5}$ enhancement to the ambient $PM_{2.5}$
332 concentration decreases from 5.40% to 3.30%. The decline of the $PM_{2.5}$
333 enhancement ratio (2.10%) is lower than that in this study (3.26%) due to the
334 continuous emission reduction after 2017. On the other hand, the ACI-induced
335 $PM_{2.5}$ enhancement decreases by 51%, from 3.96 to 1.93 $\mu\text{g m}^{-3}$. With lower
336 percentage decrease in the $PM_{2.5}$ enhancement, the ACI-induced $PM_{2.5}$
337 enhancement exceeds the ARI-induced $PM_{2.5}$ enhancement in January 2021. In
338 July, both the ARI- and ACI-induced $PM_{2.5}$ enhancements show decreasing trends,
339 the percentage decreases of the ARI-induced (31%) and ACI-induced (34%)
340 $PM_{2.5}$ enhancements are very close.

341 The contributions of the meteorological background variation and
342 anthropogenic emission reduction to the changes of the ARI- and ACI-induced
343 $PM_{2.5}$ enhancements are different. Due to the meteorological background change
344 from 2013 to 2021, the ARI- and ACI-induced $PM_{2.5}$ enhancements show
345 different characteristics in January and July. It can be seen that, the ARI-induced
346 $PM_{2.5}$ enhancement decreases from 5.59 to 3.15 $\mu\text{g m}^{-3}$ with the variation of



347 meteorological background in January, while it increases from 0.13 to 0.27 $\mu\text{g m}^{-3}$
348 $^{-3}$ in July. The primary reason for the difference is that the ambient $\text{PM}_{2.5}$
349 concentration decreases in January but increases in July caused by different
350 meteorological backgrounds. The ACI-induced $\text{PM}_{2.5}$ enhancement changes
351 slightly from 3.96 to 3.40 $\mu\text{g m}^{-3}$ in January due to the variation of meteorological
352 background. However, it increases from 2.20 to 3.31 $\mu\text{g m}^{-3}$ in July, because of
353 a large aerosol-induced LWP increase in July 2021.

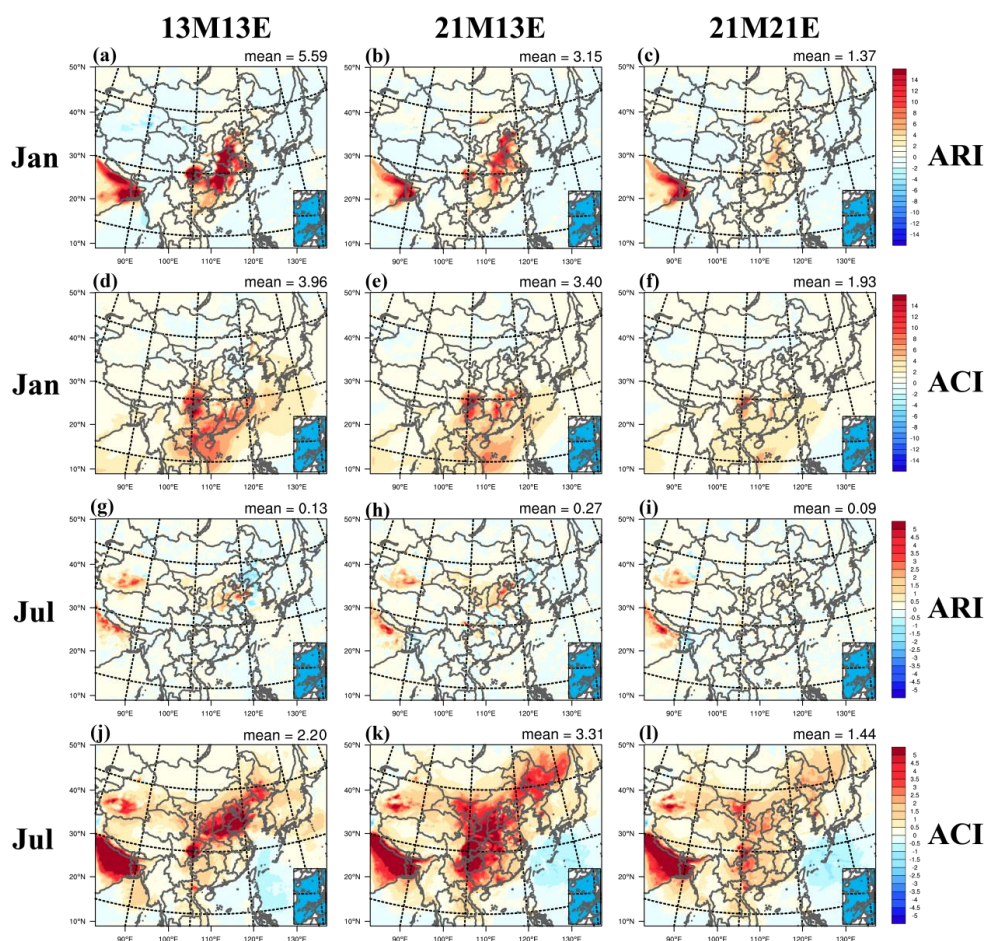
354 Considering the reduction of anthropogenic emission, the ARI- and ACI-
355 induced $\text{PM}_{2.5}$ enhancements both show declining trends (middle and right
356 columns in Fig. 2). The ARI-induced $\text{PM}_{2.5}$ enhancement decreases by 56.51% in
357 January, from 3.15 to 1.37 $\mu\text{g m}^{-3}$. The ACI-induced $\text{PM}_{2.5}$ enhancement
358 decreases by 43.24%, from 3.40 to 1.93 $\mu\text{g m}^{-3}$. The percentage decrease of the
359 ACI-induced $\text{PM}_{2.5}$ enhancement is lower than that of the ARI-induced in January,
360 which also occurs in July, when the ARI-induced $\text{PM}_{2.5}$ enhancement decreases
361 by 66.67% (from 0.27 to 0.09 $\mu\text{g m}^{-3}$) and ACI-induced $\text{PM}_{2.5}$ enhancement
362 decreases by 56.50% (from 3.31 to 1.44 $\mu\text{g m}^{-3}$).

363 In summary, both the variation of meteorological background and the
364 reduction of anthropogenic emission play important roles in changing the ARI-
365 and ACI-induced $\text{PM}_{2.5}$ enhancements. However, the decreases of ARI- and ACI-
366 induced $\text{PM}_{2.5}$ enhancements from 2013 to 2021 are primarily attributed to the
367 reduction of anthropogenic emission. In addition, the percentage decrease of the
368 ACI-induced $\text{PM}_{2.5}$ enhancement is lower than that induced by the ARI in both



369 January and July. Therefore, the ACI-induced PM_{2.5} enhancement has become
370 increasingly important in both January and July from 2013 to 2021.

371



372

373 Fig. 2. The distributions of enhanced PM_{2.5} concentrations (unit: $\mu\text{g m}^{-3}$) induced
374 by the ARI (first and third rows) and the ACI (second and fourth rows) in January
375 (first and second rows) and July (third and fourth rows) in the experiments of
376 13M13E (left column), 21M13E (middle column) and 21M21E (right column).

377

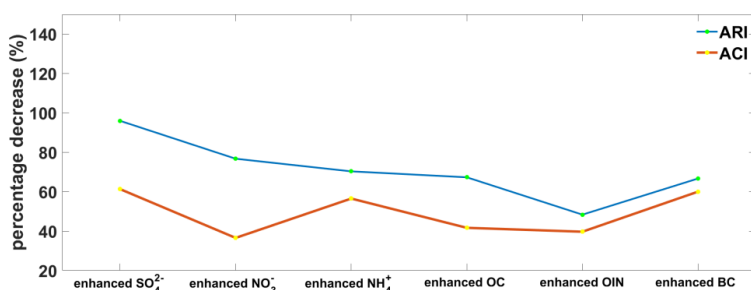


378 **3.3 The changes in the enhanced PM_{2.5} components induced by the**
379 **ARI and the ACI**

380 In terms of the anthropogenic emission reduction, the percentage decrease
381 of the ACI-induced PM_{2.5} enhancement is lower than that induced by the ARI in
382 both January and July. We find that the difference is primarily from the different
383 percentage decreases of the secondary PM_{2.5} component enhancements induced
384 by ARI and ACI.

385 Fig. 3 shows the percentage decreases of ARI- and ACI-induced PM_{2.5}
386 component enhancements caused by the anthropogenic emission reduction in
387 January and July. It can be seen that the difference between the percentage
388 decreases of the ARI- and ACI-induced enhancements of sulfate, nitrate,
389 ammonium and OC is larger than those of inorganic aerosol (OIN) and BC.
390 Specifically, the difference between the percentage decreases for sulfate, nitrate,
391 ammonium and OC enhancements are 34.66%, 40.20%, 13.80% and 25.65%
392 respectively, and the values for OIN and BC are 8.67% and 6.67%. This result
393 indicates that the lower decrease in the ACI-induced PM_{2.5} concentration
394 enhancement is mainly due to the small decrease in the ACI-induced
395 enhancements of secondary PM_{2.5} components. The main causes will be
396 illustrated in section 3.4.

397



398

399 Fig. 3. The percentage decreases (21M13E–21M21E)/21M13E) of the ARI- and
 400 ACI-induced PM_{2.5} component enhancements caused by the reduction of
 401 anthropogenic emission from 2013 to 2021.

402

403 3.4 Causes for the increased importance of ACI

404 3.4.1 Explanation from the perspective of meteorological changes

405 As discussed in previous studies, the decrease of PBLH and T2 and the
 406 increase of RH are tightly related to the ARI- and ACI-induced PM_{2.5}
 407 enhancements (Donahue et al., 2012; Ding et al., 2016; Moch et al., 2022; Liu et
 408 al., 2018). From the perspective of the ARI- and ACI-induced changes in
 409 meteorological factors, we investigate the primary reasons for the increasing
 410 importance of the ACI-induced PM_{2.5} enhancement under the reduction of
 411 anthropogenic emission.

412 Fig. 4 shows the percentage decreases of ARI- and ACI-induced decrease of
 413 SWDOWN, PBLH and T2 and increase of RH due to the reduction of
 414 anthropogenic emission from 2013 to 2021. In January, in order to illustrate the
 415 reasons of the lower percentage decrease in the ACI-induced PM_{2.5} enhancement



416 clearly, we take the highly polluted NCP region as an example. As shown in Fig.
417 4c, the percentage decreases of the ACI-induced decline of SWDOWN (19%),
418 PBLH (27%) and T2 (20%) and the increase of RH (24%) are lower than those
419 of the ARI-induced decline of SWDOWN (29%), PBLH (39%) and T2 (32%) and
420 the increase of RH (36%). The phenomenon in July is similar with that in January
421 (Figs. 4a and b). To our knowledge, the PBLH and T2 are determined by the
422 incoming solar radiation at the surface, and they can strongly influence the RH.
423 So the lower percentage decrease in the ACI-induced reductions of PBLH and T2
424 and increase of RH could be explained by the lower percentage decrease in the
425 ACI-induced SWDOWN reduction.

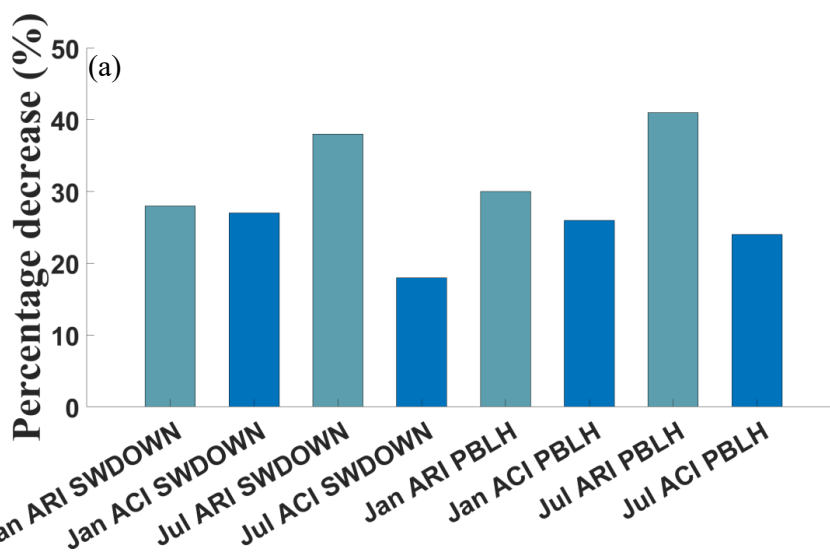
426 We believe that the relatively lower decrease in the ACI-induced SWDOWN
427 reduction is inevitable under high ambient $PM_{2.5}$ concentration. As shown in Fig.
428 S5, the SWDOWN reduction induced by the ARI shows a linear relationship with
429 the decline of ambient $PM_{2.5}$ concentration, which is similar with Zhou et al.
430 (2018). In contrast, the decrease in the SWDOWN reduction induced by the ACI
431 is lower than that by the ARI due to the ambient $PM_{2.5}$ decrease in the high $PM_{2.5}$ -
432 polluted regime. The reason is that the decrease in the ambient $PM_{2.5}$
433 concentration directly weakens the ARI-induced SWDOWN reduction, but it has
434 minor impact on the ACI-induced LWP and cloud effective radius (R_e) because
435 high ambient $PM_{2.5}$ concentration still provides enough CCN (Gryspeerd et al.,
436 2019; Yang et al., 2019; Liu et al., 2020). Note that when the ambient $PM_{2.5}$
437 concentration decreases to $20 \mu\text{g m}^{-3}$, the weakening of SWDOWN reduction



438 induced by the ACI might be larger than that by the ARI, because the decrease in
439 ambient $PM_{2.5}$ concentration will reduce the CCN under the $PM_{2.5}$ -clean
440 condition, which will reduce CF, cloud water content and increase Re (Yang et
441 al., 2019; Liu et al., 2020).

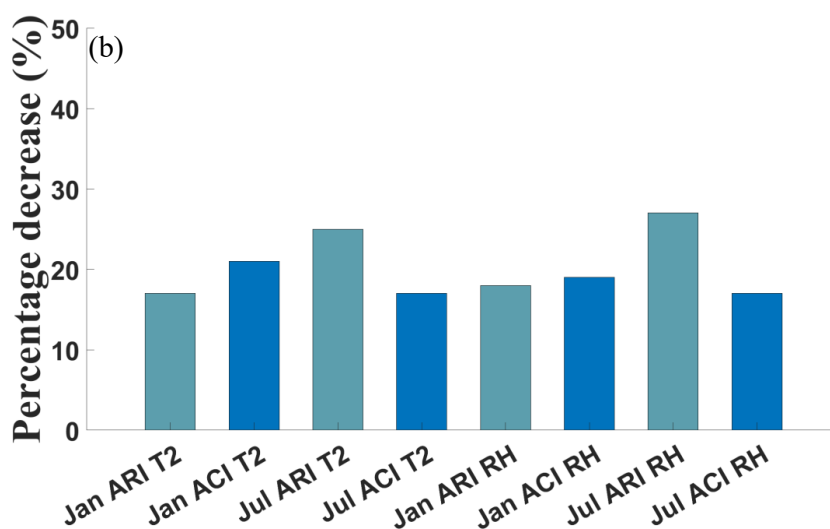
442 Especially, the lower PBLH caused by ARI and ACI will enhance the
443 accumulation of all the $PM_{2.5}$ components, but higher RH and lower T2 induced
444 by the ARI and ACI could promote the production of extra secondary $PM_{2.5}$
445 components through strengthening aqueous and heterogeneous reactions and
446 causing gas precursors to condense into particle matter (Donahue et al., 2012; Liu
447 et al., 2018). Therefore, lower percentage decrease in the T2 reduction and RH
448 increase induced by the ACI is more likely to weaken the decrease in the
449 enhancements of secondary $PM_{2.5}$ components. This well explains the lower
450 percentage decreases in the enhancements of secondary $PM_{2.5}$ components
451 induced by the ACI than those by the ARI as shown in Fig. 3.

452

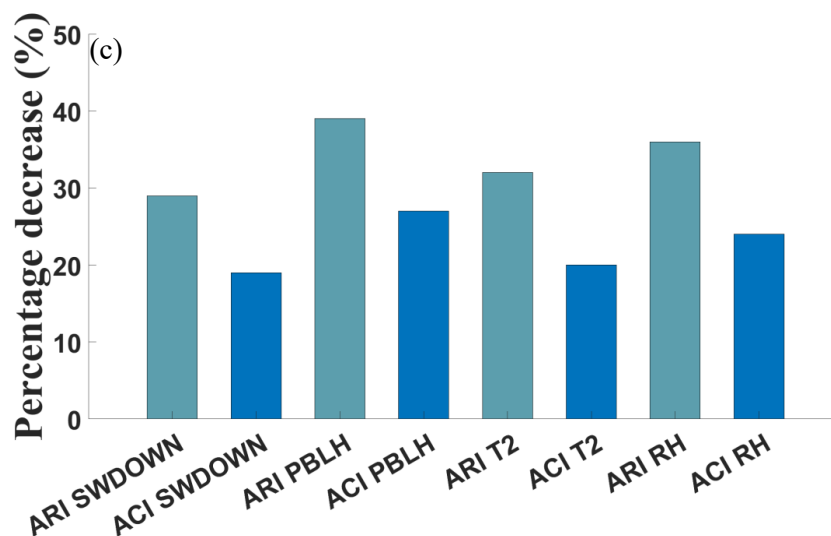


453

454



455



456

457 Fig. 4. The percentage decreases of the regional averages of (a) the decrease of
458 SWDOWN and PBLH, and (b) the T2 reduction and RH increase induced by ARI
459 and ACI in eastern China caused by the anthropogenic emission reduction in
460 January and July from 2013 to 2021. (c) is the same as (a) and (b), but in the NCP
461 region in January.

462

463 3.4.2 Explanation from the perspective of PM_{2.5} concentration distribution 464 changes

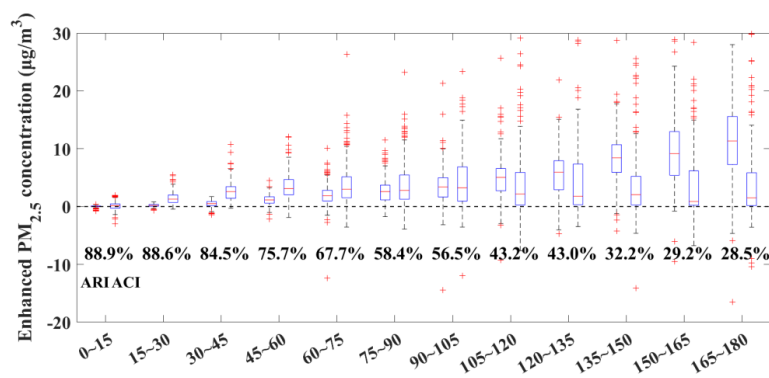
465 Ambient PM_{2.5} concentration is the fundamental factor to trigger the ARI
466 and the ACI. In order to further explore the reasons for the increasing importance
467 of enhanced PM_{2.5} concentration induced by ACI, we discuss the characteristics
468 of enhanced PM_{2.5} concentration induced by ARI and ACI under different PM_{2.5}
469 pollution levels.

470 The PM_{2.5} concentration is divided into 12 levels from 0 to 180 $\mu\text{g m}^{-3}$. As

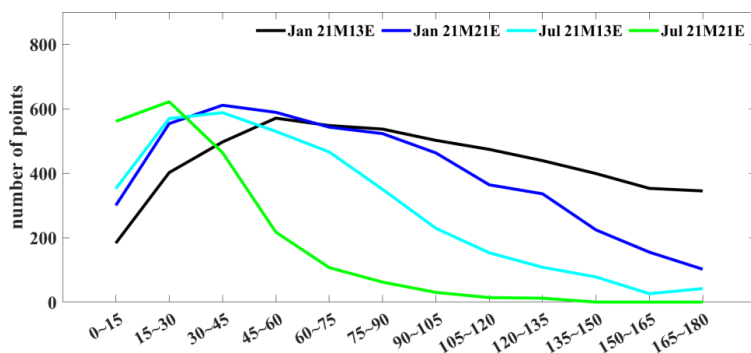


471 shown in Fig. 5a, under the heavy PM_{2.5}-polluted regime (135–180 μg m⁻³), the
 472 enhanced PM_{2.5} induced by the ARI is much larger than that by the ACI, while
 473 the ACI-induced PM_{2.5} enhancement will obviously exceed the ARI-induced
 474 PM_{2.5} enhancement in the PM_{2.5}-clean condition (0–45 μg m⁻³). It indicates the
 475 fast decrease in the ARI-induced PM_{2.5} enhancement and the increasing
 476 contribution of the ACI-induced enhancement with the decrease of PM_{2.5}
 477 concentration. As illustrated in section 3.4.1, the lower percentage decrease in the
 478 ACI-induced PM_{2.5} enhancement with the decrease of PM_{2.5} concentration is
 479 because of the lower percentage decrease in the ACI-induced SWDOWN
 480 reduction, which is due to the lower decrease in the LWP caused by the ambient
 481 PM_{2.5} decrease in the heavy PM_{2.5}-polluted regime. Considering the decrease in
 482 the ambient PM_{2.5} concentration due to the anthropogenic emission reduction
 483 from 2013 to 2021 (Fig. 5b), the ACI-induced PM_{2.5} enhancement certainly
 484 contributes more to the total PM_{2.5} concentration in 2021.

485



486



487

488 Fig. 5. (a) The enhanced PM_{2.5} concentrations induced by ARI and ACI under
 489 different ambient PM_{2.5} levels. The percentage represents the ratio of the ACI-
 490 induced PM_{2.5} enhancement to the sum of ARI- and ACI-induced PM_{2.5}
 491 enhancements. (b) The distributions of ambient PM_{2.5} levels in January and July
 492 in the experiments of 21M13E and 21M21E.

493

494 4. Conclusions

495 Under the background of sharp anthropogenic emission reduction, this
 496 study investigates changes of the ARI- and ACI-induced PM_{2.5} enhancements for
 497 2013–2021, and explores the causes for these changes from the perspectives of
 498 meteorological factors and PM_{2.5} concentration distribution.

499 The results show that the enhanced PM_{2.5} induced by the ARI (5.59 µg m⁻³)
 500 is greater than that by the ACI (3.96 µg m⁻³) in January 2013. However, the ARI-
 501 and ACI-induced PM_{2.5} enhancements decrease from 5.59 and 3.96 µg m⁻³ to 1.37
 502 and 1.93 µg m⁻³ in January and decrease by 75% and 51% for 2013–2021. The
 503 smaller decrease ratio (51%) for ACI-induced PM_{2.5} enhancements implies that

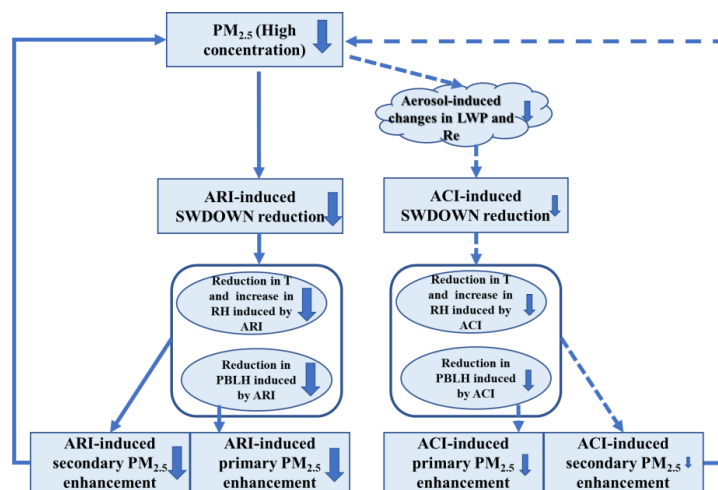


504 ACI becomes more important for enhancing $PM_{2.5}$ concentrations in January
505 2021. Furthermore, we separated the contributions of meteorological background
506 variation and anthropogenic emission reduction. Compared with the
507 meteorological background variation, anthropogenic emission reduction plays a
508 more important role in causing the decrease of ARI- and ACI-induced $PM_{2.5}$
509 enhancements. Owing to only emission reduction, the enhanced $PM_{2.5}$
510 concentrations induced by the ARI and ACI decrease by 56% and 43% in January
511 and 66% and 56% in July, respectively. The ACI-induced $PM_{2.5}$ enhancement
512 becomes increasingly important in both January and July for 2013–2021. More
513 specifically, the lower percentage decrease in the ACI-induced $PM_{2.5}$
514 enhancement is dominated by the lower decrease in the enhancements of
515 secondary $PM_{2.5}$ components.

516 The lower percentage decrease in the enhanced $PM_{2.5}$ induced by the ACI is
517 due to the lower percentage decrease in the ACI-induced SWDOWN reduction,
518 which is because of the lower decrease in the LWP and increase in the Re caused
519 by the ambient $PM_{2.5}$ decrease in the high $PM_{2.5}$ -polluted regime (Fig. 6). At the
520 same time, the lower percentage decreases in the T2 reduction and RH increase
521 induced by the ACI further lead to the lower percentage decrease in the
522 enhancements of the ACI-induced secondary $PM_{2.5}$ components (Fig. 6). Notably,
523 due to relative lower percentage decrease in the ACI-induced SWDOWN
524 reduction in the high $PM_{2.5}$ -polluted regime, the increasing importance of ACI-
525 induced $PM_{2.5}$ enhancement is a matter of course with the ambient $PM_{2.5}$ decrease.



526



527

528

529

530

531

532

533

534

535

536

537

538

539

540

541

Fig. 6. Schematic diagram for the decrease of ARI- and ACI-induced primary and secondary $PM_{2.5}$ enhancement due to reduction in ambient $PM_{2.5}$ concentration. Solid arrows represent these processes are strongly weakened; dotted arrows represent these processes are slightly weakened.

This study has important implication for the $PM_{2.5}$ control. As we know, ARI- and ACI-induced $PM_{2.5}$ enhancements have a non-negligible contribution to the deterioration of $PM_{2.5}$ air quality. Previous research has investigated the impact of anthropogenic emission reduction on the ARI-induced $PM_{2.5}$ enhancement (Zhou et al., 2019). But compared with $PM_{2.5}$ enhancement induced by ARI, that induced by ACI is more complicated and harder to be alleviated. Our findings have further revealed that the ACI-induced $PM_{2.5}$ enhancement is getting more important relative to that induced by ARI. This is especially true in cloud-prone areas like Sichuan-Chongqing area, which have witnessed rather weak



542 decreases of ACI-induced $PM_{2.5}$ concentration in the past decade due to weak
543 decreases of aerosol-induced LWP under the condition of high ambient $PM_{2.5}$
544 level (Fig. 2). The ACI-induced $PM_{2.5}$ enhancement needs to be considered more
545 seriously in the formulation of control policies to meet national $PM_{2.5}$ air
546 quality standard, especially in cloud-prone areas with high ambient $PM_{2.5}$
547 concentration.

548

549 **Data and Code availability.**

550 The data and code used in this study are available upon request from Da Gao
551 (dagao94@foxmail.com).

552

553 **Author Contribution**

554 D.G., B.Z. and S.W. designed the research; D.G., B.Z., J.S. and B.G. improved
555 the WRF-Chem performance; D.G. and B.Z. further developed WRF-Chem and
556 performed the simulations; X.W., S.L. and Z.D. provide the anthropogenic
557 emissions; D.G. analyzed the data with the help from B.Z., S.W. and Y.W.; D.Y.
558 and J.S. help D.G. to design some figures; S.W., Y.W., Y.Z. and Y.H. presented
559 important suggestions for the analysis and writings; D.G. and B.Z. wrote the
560 paper with inputs from all co-authors.

561

562 **Competing interests**

563 The author declares no competing interests.



564

565 **Acknowledgments.**

566 This research is supported by the National Key Research and Development
567 Program of China (2022YFC3701000, Task 5), the National Natural Science
568 Foundation of China (22188102), and the Tencent Foundation through the
569 XPLOER PRIZE.

570

571 **References**

572 Abdul-Razzak, H., Ghan, S.J., A parameterization of aerosol activation - 3.
573 Sectional representation, *J Geophys Res-Atmos* 107(2002).

574 Bellouin, N. et al., Bounding Global Aerosol Radiative Forcing of Climate
575 Change, *Rev Geophys* 58(2020).

576 Bennartz, R., Global assessment of marine boundary layer cloud droplet number
577 concentration from satellite, *J Geophys Res-Atmos* 112(2007).

578 Bougeault, P., Lacarrere, P., Parameterization Of Orography-Induced Turbulence
579 In a Mesobeta-Scale Model, *Mon Weather Rev* 117(1989), pp. 1872-1890.

580 Carter, W., Documentation of the SAPRC-99 Chemical Mechanism for VOC
581 Reactivity Assessment. (2000).

582 Ding, A.J. et al., Enhanced haze pollution by black carbon in megacities in China,
583 *Geophys Res Lett* 43(2016), pp. 2873-2879.

584 Ding, D., Xing, J., Wang, S.X., Liu, K.Y., Hao, J.M., Estimated Contributions of
585 Emissions Controls, Meteorological Factors, Population Growth, and



586 Changes in Baseline Mortality to Reductions in Ambient PM_{2.5} and PM_{2.5}-
587 Related Mortality in China, 2013-2017, *Environ Health Persp* 127(2019).
588 Donahue, N.M. et al., Aging of biogenic secondary organic aerosol via gas-phase
589 OH radical reactions, *P Natl Acad Sci USA* 109(2012), pp. 13503-13508.
590 Emery, C., Tai, E., Yarwood, G. , Enhanced meteorological modeling and
591 performance evaluation for two texas episodes. Report to the Texas Natural
592 Resources Conservation Commission (2001).
593 Fan, J.W., Wang, Y., Rosenfeld, D., Liu, X.H., Review of Aerosol-Cloud
594 Interactions: Mechanisms, Significance, and Challenges, *J Atmos Sci*
595 73(2016), pp. 4221-4252.
596 Fast, J.D. et al., Evolution of ozone, particulates, and aerosol direct radiative
597 forcing in the vicinity of Houston using a fully coupled meteorology-
598 chemistry-aerosol model, *J Geophys Res-Atmos* 111(2006).
599 Forkel, R. et al., Analysis of the WRF-Chem contributions to AQMEII phase2
600 with respect to aerosol radiative feedbacks on meteorology and pollutant
601 distributions, *Atmos Environ* 115(2015), pp. 630-645.
602 Forkel, R. et al., Effect of aerosol-radiation feedback on regional air quality - A
603 case study with WRF/Chem, *Atmos Environ* 53(2012), pp. 202-211.
604 Forster, P., T. Storelvmo, K. Armour, W. Collins, J.-L. Dufresne, D. Frame, D.J.
605 Lunt, T. Mauritsen, M.D. Palmer, M. Watanabe, M. Wild, and H. Zhang, The
606 Earth's Energy Budget, Climate Feedbacks, and Climate Sensitivity. In
607 *Climate Change 2021: The Physical Science Basis. Contribution of Working*



- 608 Group I to the Sixth Assessment Report of the Intergovernmental Panel on
609 Climate Change [Masson-Delmotte, V., P. Zhai, A. Pirani, S.L. Connors, C.
610 Péan, S. Berger, N. Caud, Y. Chen, L. Goldfarb, M.I. Gomis, M. Huang,
611 K. Leitzell, E. Lonnoy, J.B.R. Matthews, T.K. Maycock, T. Waterfield, O.
612 Yelekçi, R. Yu, and B. Zhou (eds.)]. Cambridge, United Kingdom and New
613 York, NY, USA, Cambridge University Press (2021), pp. 923–1054.
- 614 Gao, M. et al., Air quality and climate change, Topic 3 of the Model Inter-
615 Comparison Study for Asia Phase III (MICS-Asia III) - Part 2: aerosol
616 radiative effects and aerosol feedbacks, *Atmos Chem Phys* 20(2020), pp.
617 1147-1161.
- 618 Gong, W. et al., Modelling aerosol-cloud-meteorology interaction: A case study
619 with a fully coupled air quality model (GEM-MACH), *Atmos Environ*
620 115(2015), pp. 695-715.
- 621 Grell, G.A., Freitas, S.R., A scale and aerosol aware stochastic convective
622 parameterization for weather and air quality modeling, *Atmos Chem Phys*
623 14(2014), pp. 5233-5250.
- 624 Gryspeerdt, E. et al., Constraining the aerosol influence on cloud liquid water
625 path, *Atmos Chem Phys* 19(2019), pp. 5331-5347.
- 626 Guenther, A. et al., Estimates of global terrestrial isoprene emissions using
627 MEGAN (Model of Emissions of Gases and Aerosols from Nature), *Atmos*
628 *Chem Phys* 6(2006), pp. 3181-3210.
- 629 Gustafson, W.I., Chapman, E.G., Ghan, S.J., Easter, R.C., Fast, J.D., Impact on



630 modeled cloud characteristics due to simplified treatment of uniform cloud
631 condensation nuclei during NEAQS 2004, *Geophys Res Lett* 34(2007).

632 Hong, C.P. et al., Weakening aerosol direct radiative effects mitigate climate
633 penalty on Chinese air quality, *Nat Clim Change* 10(2020), pp. 845-+.

634 Iacono, M.J. et al., Radiative forcing by long-lived greenhouse gases:
635 Calculations with the AER radiative transfer models, *J Geophys Res-Atmos*
636 113(2008).

637 Janjic, Z.I., The Step-Mountain Eta Coordinate Model - Further Developments
638 Of the Convection, Viscous Sublayer, And Turbulence Closure Schemes,
639 *Mon Weather Rev* 122(1994), pp. 927-945.

640 Kong, X. et al., Analysis of meteorology-chemistry interactions during air
641 pollution episodes using online coupled models within AQMEII phase-2,
642 *Atmos Environ* 115(2015), pp. 527-540.

643 Le, T.H. et al., Unexpected air pollution with marked emission reductions during
644 the COVID-19 outbreak in China, *Science* 369(2020), pp. 702-+.

645 Li, M. et al., MIX: a mosaic Asian anthropogenic emission inventory under the
646 international collaboration framework of the MICS-Asia and HTAP, *Atmos*
647 *Chem Phys* 17(2017), pp. 935-963.

648 Li S.Y., Wang S.X., Wu Q.R., Emission trends of air pollutants and CO₂ in China
649 from 2005 to 2021, *Earth System Science Data Discussion*(2023).

650 Liu, L.X. et al., Impact of biomass burning aerosols on radiation, clouds, and
651 precipitation over the Amazon: relative importance of aerosol-cloud and



- 652 aerosol-radiation interactions, *Atmos Chem Phys* 20(2020), pp. 13283-
653 13301.
- 654 Liu, Q. et al., New positive feedback mechanism between boundary layer
655 meteorology and secondary aerosol formation during severe haze events, *Sci*
656 *Rep-Uk* 8(2018).
- 657 Liu, S. et al., Understanding of Aerosol-Climate Interactions in China: Aerosol
658 Impacts on Solar Radiation, Temperature, Cloud, and Precipitation and Its
659 Changes Under Future Climate and Emission Scenarios, *Curr Pollut Rep*
660 5(2019), pp. 36-51.
- 661 Moch, J.M. et al., Aerosol-Radiation Interactions in China in Winter: Competing
662 Effects of Reduced Shortwave Radiation and Cloud-Snowfall-Albedo
663 Feedbacks Under Rapidly Changing Emissions, *J Geophys Res-Atmos*
664 127(2022).
- 665 Morrison, H., Thompson, G., Tatarskii, V., Impact of Cloud Microphysics on the
666 Development of Trailing Stratiform Precipitation in a Simulated Squall Line:
667 Comparison of One- and Two-Moment Schemes, *Mon Weather Rev*
668 137(2009), pp. 991-1007.
- 669 Niu, G.Y. et al., The community Noah land surface model with
670 multiparameterization options (Noah-MP): 1. Model description and
671 evaluation with local-scale measurements, *J Geophys Res-Atmos* 116(2011).
- 672 Rosenfeld, D., Sherwood, S., Wood, R., Donner, L., Climate Effects of Aerosol-
673 Cloud Interactions, *Science* 343(2014), pp. 379-380.



- 674 Seinfeld, J.H. et al., Improving our fundamental understanding of the role of
675 aerosol-cloud interactions in the climate system, P Natl Acad Sci USA
676 113(2016), pp. 5781-5790.
- 677 Shrivastava, M. et al., Modeling organic aerosols in a megacity: comparison of
678 simple and complex representations of the volatility basis set approach,
679 Atmos Chem Phys 11(2011), pp. 6639-6662.
- 680 Wang, H. et al., Mesoscale modelling study of the interactions between aerosols
681 and PBL meteorology during a haze episode in China Jing-Jin-Ji and its near
682 surrounding region - Part 2: Aerosols' radiative feedback effects, Atmos
683 Chem Phys 15(2015), pp. 3277-3287.
- 684 Wang, J.D. et al., Impact of aerosol-meteorology interactions on fine particle
685 pollution during China's severe haze episode in January 2013, Environ Res
686 Lett 9(2014).
- 687 Wang, J.D. et al., Particulate matter pollution over China and the effects of control
688 policies, Sci Total Environ 584(2017), pp. 426-447.
- 689 Wang, Y.S. et al., Trends in particulate matter and its chemical compositions in
690 China from 2013-2017, Sci China Earth Sci 62(2019), pp. 1857-1871.
- 691 Wang, Z.F., Li, J., Wang, Z., Yang, W., Tang, X., Ge, B., Yan,P., Zhu, L., Chen,
692 X., and Chen, H., Modeling study of regional severe hazes over mid-eastern
693 China in January 2013 and its implications on pollution prevention and
694 control, Science China Earth Sciences(2014), pp. 3-13.
- 695 Wild, O., Zhu, X., Prather, M.J., Fast-j: Accurate simulation of in- and below-



- 696 cloud photolysis in tropospheric chemical models, *J Atmos Chem* 37(2000),
697 pp. 245-282.
- 698 Wu, J.R. et al., Aerosol-photolysis interaction reduces particulate matter during
699 wintertime haze events, *P Natl Acad Sci USA* 117(2020), pp. 9755-9761.
- 700 Xiong, C.R., Li, J., Liu, Z.X., Zhang, Z.Y., The dominant role of aerosol-cloud
701 interactions in aerosol-boundary layer feedback: Case studies in three
702 megacities in China, *Front Env Sci-Switz* 10(2022).
- 703 Yang, Y. et al., Toward understanding the process-level impacts of aerosols on
704 microphysical properties of shallow cumulus cloud using aircraft
705 observations, *Atmos Res* 221(2019), pp. 27-33.
- 706 Zaveri, R.A., Easter, R.C., Fast, J.D., Peters, L.K., Model for Simulating Aerosol
707 Interactions and Chemistry (MOSAIC), *J Geophys Res-Atmos* 113(2008).
- 708 Zhang, B., Wang, Y., Hao, J., Simulating aerosol-radiation-cloud feedbacks on
709 meteorology and air quality over eastern China under severe haze conditions
710 in winter, *Atmos Chem Phys* 15(2015), pp. 2387-2404.
- 711 Zhang, F. et al., An unexpected catalyst dominates formation and radiative forcing
712 of regional haze, *P Natl Acad Sci USA* 117(2020), pp. 3960-3966.
- 713 Zhang, F.F. et al., Role of black carbon in modulating aerosol direct effects driven
714 by air pollution controls during 2013-2017 in China, *Sci Total Environ*
715 832(2022).
- 716 Zhang, X. et al., Enhancement of PM_{2.5} Concentrations by Aerosol-Meteorology
717 Interactions Over China, *J Geophys Res-Atmos* 123(2018), pp. 1179-1194.



- 718 Zhao, B. et al., Enhanced PM_{2.5} pollution in China due to aerosol-cloud
719 interactions, *Sci Rep-Uk* 7(2017).
- 720 Zhao, C. et al., Uncertainty in modeling dust mass balance and radiative forcing
721 from size parameterization, *Atmos Chem Phys* 13(2013), pp. 10733-10753.
- 722 Zhao, C. et al., The spatial distribution of mineral dust and its shortwave radiative
723 forcing over North Africa: modeling sensitivities to dust emissions and
724 aerosol size treatments, *Atmos Chem Phys* 10(2010), pp. 8821-8838.
- 725 Zheng, H.T. et al., Development of a unit-based industrial emission inventory in
726 the Beijing-Tianjin-Hebei region and resulting improvement in air quality
727 modeling, *Atmos Chem Phys* 19(2019), pp. 3447-3462.
- 728 Zhou, M. et al., The impact of aerosol-radiation interactions on the effectiveness
729 of emission control measures, *Environ Res Lett* 14(2019).